Fatigue life evaluation of metallic structures under multiaxial random loading

Fatigue life evaluation of metallic structures under multiaxial random loading

Andrea Carpinteri

Giovanni Fortese

Camilla Ronchei

Daniela Scorza

Andrea Spagnoli

Sabrina Vantadori*

sabrina.vantadori@unipr.it

Department of Civil-Environmental Engineering & Architecture, University of Parma, Parco Area delle Scienze 181/A, 43124 Parma, Italy

*Corresponding author.

Abstract

A frequency-domain critical-plane criterion is reformulated in order to improve its accuracy in terms of fatigue life estimation for smooth metallic structural components under multiaxial random loading. The criterion here proposed consists of three steps: (i) definition of the critical plane; (ii) Power Spectral Density (PSD) evaluation of an equivalent normal stress; (iii) estimation of fatigue life by implementing damage models different from that used in the original formulation. Such a reformulated criterion is numerically validated by employing experimental fatigue results for 18G2A and 10HNAP structural steels, subjected to random combined bending and torsion. Further, the above theoretical results are also compared with those determined through a time-domain criterion proposed in the past by some of the present authors.

Keywords: Critical plane approach; Fatigue life evaluation; Frequency domain; Multiaxial random loading; Time domain

Nomenclature

C

coefficient of the normal stress S–N curve

$E[D_{NB}]$

expected fatigue damage per unit time by employing the narrow-band approximation

$E[D_{RC}]$

expected fatigue damage per unit time by employing the range-mean counting method

$E[D_{RFC}]$

expected fatigue damage per unit time by employing the rain-flow counting method

k

inverse slope of the normal stress S–N curve

$p_a(s)$

marginal probability distribution of the amplitude (s) of the $\{X(t)\}$ counted cycles of loading

$p_p(X)$

probability distribution of peaks of $\{X(t)\}$

PSD

Power Spectral Density

$PXYZ$

fixed frame

$PX'Y'Z'$

rotated coordinate system

$P\hat{1}\hat{2}\hat{3}$

reference system of the weighted mean principal stress axes

$Puvw$

reference system attached to the critical plane

$S_{eq}(\omega)$

equivalent PSD function

$\mathbf{s}_{xyz}(t)$

stress vector referred to the reference system $PXYZ$

$\mathbf{s}_{x'y'z'}(t)$

stress vector referred to the reference system $PX'Y'Z'$

$\mathbf{s}_{uvw}(t)$

stress vector referred to the reference system $Puvw$

$S_{X,X}(\omega)$

two-sided PSD function of $\{X(t)\}$

$\mathbf{S}_{xyz}(\omega)$

PSD matrix of $\mathbf{s}_{xyz}(t)$

$S_{i,j}(\omega)$

coefficients of the $\mathbf{S}_{xyz}(\omega)$ matrix

$\mathbf{S}_{x'y'z'}(\omega)$

PSD matrix of $\mathbf{s}_{x'y'z'}(t)$

$S_{i',j'}(\omega)$

coefficients of the $\mathbf{S}_{x'y'z'}(\omega)$ matrix

$S_{3',3'}$

PSD function of the normal stress $\sigma_{z'}$

$S_{6',6'}$

PSD function of the shear stress $\tau_{y'z'}$

$\mathbf{S}_{uvw}(\omega)$

PSD matrix of $\mathbf{s}_{uvw}(t)$

$S_{3'',3''}$

PSD function of the normal stress σ_{w}

$S_{6'',6''}$

PSD function of the shear stress τ_{vw}

t

time

T

observation time interval

T_{cal}

calculated fatigue life

T_{exp}

experimental fatigue life

$\{X(t)\}$

one-dimensional ergodic stationary stochastic process

α_n

n-th bandwidth parameter, with n positive real number

α_2

regularity index

γ

rotation about w -axis

δ

angle between the averaged direction $\hat{\mathbf{i}}$ and the normal $\mathbf{w}$ to the critical plane (Fig. 4)

λ_n

n-th spectral moment, with n positive real number

μ_X

mean value of $\{X(t)\}$

ν_a

expected rate of occurrence of cycles of $\{X(t)\}$

$\nu^+_{\mu_X}$

expected rate of mean-upcrossings of $\{X(t)\}$

ν_p

expected rate of occurrence of peaks of $\{X(t)\}$

ν^+_0

expected rate of zero-upcrossings of $\sigma_{z'}$

$\sigma_{af,-1}$

normal stress fatigue limit for fully reversed normal stress (loading ratio $R=-1$)

σ^2_X

variance of the process $\{X(t)\}$

$\sigma^2_{\dot{X}}$

variance of the first derivative of the process $\{X(t)\}$

$\sigma^2_{\ddot{X}}$

variance of the second derivative of the process $\{X(t)\}$

$\tau_{af,-1}$

shear stress fatigue limit for fully reversed shear stress (loading ratio $R=-1$)

ϕ, θ, ψ

Euler angles

ω

pulsation

1 Introduction

The fatigue design of engineering components subjected to time-varying loading characterised by random amplitudes is a complex issue [1–4], especially when the local stress state is multiaxial [5–10].

The procedures usually employed to perform life evaluations of structural components under random fatigue loading are formulated in time domain or, alternatively, in frequency domain. Time-domain procedures are based on cycle counting methods and damage accumulation rules [11–14]. In order to obtain reliable statistical parameters of the loading process, the time histories (experimentally measured on the real structural component being examined) of the local stress or strain tensor components are required, and many records are needed.

On the other hand, frequency-domain procedures for random loading need the cycle distribution from a statistical point-of-view: as a matter of fact, starting from the Power Spectral Density (PSD) function of local stress or strain tensor components, damage can directly be evaluated [15–20].

Note that, in both time- and frequency-domain procedures, damage evaluation is affected by the uncertainty related to the algorithm used to count the loading cycles. Note that a cycle counting method is not always required: for example, it is not needed for the Event Independent Cumulative Damage (EVICD) fatigue prediction model, that takes the plastic strain energy as the major contributor to the fatigue damage [21].

When a cycle counting method is needed, the Rain-Flow Counting procedure [22], proposed for deterministic loading, is considered as the most accurate method by the scientific community. Strong efforts have been made in many research works to describe the statistical distribution of rain-flow loading cycles, since the rain-flow amplitude distribution is not known in exact manner.

Therefore, in order to evaluate how the procedure employed to count cycles influences fatigue life estimation, the original frequency-domain criterion proposed by the authors in Ref. [20] is reformulated here by implementing different counting procedures [23–25]. In particular, the present criterion consists of the following three steps:

(i) definition of the critical plane;

(ii) PSD evaluation of an equivalent normal stress;

(iii) estimation of fatigue life.

In more detail: (i) the critical plane is proposed to be dependent on the PSD matrix of the stress tensor; (ii) on such a critical plane (verification plane), the PSD of an equivalent stress is defined by a linear combination of the PSD functions of both normal stress and shear stress, the latter projected along the direction that maximises the variance of such a stress; (iii) the PSD of the above equivalent stress is used to estimate fatigue damage and to compute the fatigue life of the structural component being examined.

The criterion is numerically validated by analysing some relevant random fatigue experimental results [26] related to 18G2A and 10HNAP structural steels, under non-proportional random bending and torsion stresses. As a matter of fact, such a case is quite significant in many mechanical and structural components subjected to random multiaxial loading in service, where a fatigue life reduction due to non-proportional loading is observed [27].

Finally, the capabilities of the present criterion are also highlighted by comparing the above theoretical results with those determined through a time-domain criterion proposed in the past by some of the authors [13,14].

2 One-dimensional stochastic process: theoretical background

Several engineering structures are subjected to loads, such as those due to traffic, wind, waves, vibrations, which can be described as ergodic and stationary stochastic processes. Such processes are those commonly used for cyclic loading in order to handle fatigue calculations in the frequency domain.

Now let us consider a one-dimensional ergodic stationary stochastic sampled process $\{X(t)\}$, whose two-sided Power Spectral Density (PSD) function is indicated by $S_{X,X}(\omega)$. Such a PSD function fully describes the stochastic process in the time domain. The *n*-order spectral moments of the PSD function $S_{X,X}(\omega)$ are defined as follows:

$$\lambda_n = \int_{-\infty}^{+\infty} |\omega|^n S_{X,X}(\omega) d\omega \tag{1}$$

As is well-known, there exist correlations between such moments and σ_X^2 (variance of $\{X(t)\}$), $\sigma_{\dot{X}}^2$ and $\sigma_{\ddot{X}}^2$ (variances of $\{\dot{X}(t)\}$ and $\{\ddot{X}(t)\}$, which are derivatives of the process $\{X(t)\}$):

$$\lambda_0 = \sigma_X^2 \tag{2a}$$

$$\lambda_2 = \sigma_{\dot{X}}^2 \tag{2b}$$

$$\lambda_4 = \sigma_{\dot{X}}^2 \tag{2c}$$

Provided that the ergodic stationary stochastic process $\{X(t)\}$ is Gaussian, the number of crossing with positive slope of the mean value (μ_X) per unit time, $\nu_{\mu_X}^+$, can be obtained from the spectral moments λ_0 and λ_2 of $S_{XX}(\omega)$:

$$\nu_{\mu_X}^+ = \frac{1}{2\pi}\sqrt{\frac{\lambda_2}{\lambda_0}} \tag{3}$$

whereas the rate of number of peaks, ν_p , can be obtained from the spectral moments λ_2 and λ_4 of $S_{XX}(\omega)$ as follows:

$$\nu_p = \frac{1}{2\pi}\sqrt{\frac{\lambda_4}{\lambda_2}} \tag{4}$$

From the spectral moments of the PSD function $S_{XX}(\omega)$, we can compute the bandwidth parameters, α_n , which describe the shape and the geometrical frequency distribution of $S_{XX}(\omega)$, namely:

$$\alpha_n = \frac{\lambda_n}{\sqrt{\lambda_0 \lambda_{2n}}} \tag{5}$$

The most common bandwidth parameter is α_2 ($n = 2$), named regularity index (if the stochastic process is narrow-band type, such a parameter tends to the unity, whereas it tends to zero in the case of broad-band process). As an example, two single modal PSD functions of narrow and wide bandwidth processes with the corresponding time-history fragments are illustrated in Fig. 1.

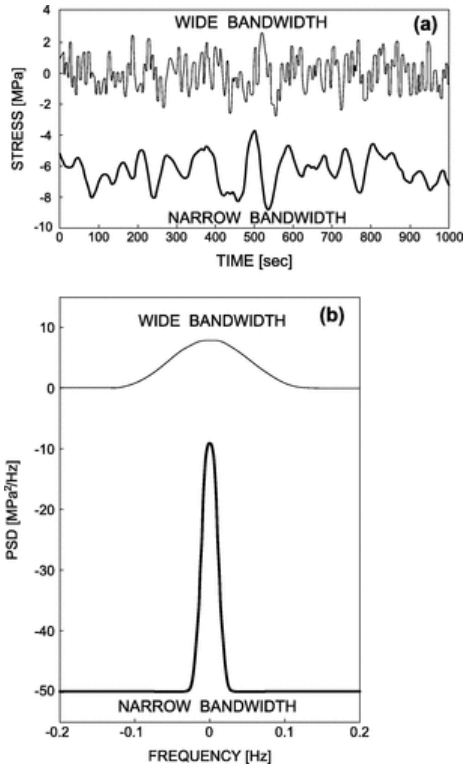

Fig. 1 Example of narrow- and broad-band processes: (a) signals; (b) PSD functions.

If the ergodic stationary Gaussian stochastic process $\{X(t)\}$ has a zero mean value, the probability distribution of peaks, $p_p(X)$, is given by:

$$p_p(X) = \frac{\sqrt{1-\alpha_2^2}}{\sqrt{2\pi}\sigma_X} e^{-\frac{X^2}{2\sigma_X^2(1-\alpha_2^2)}} + \frac{\alpha_2 X}{\sigma_X^2} e^{-\frac{X^2}{2\sigma_X^2}} \phi\left(\frac{\alpha_2 X}{\sigma_X\sqrt{1-\alpha_2^2}}\right) \quad (6a)$$

where the operator $\phi(.)$ is a standard normal distribution function that, for a generic stochastic process $\{x(t)\}$, operates as follows:

$$\phi(x) = \frac{2}{\pi}\int_{-\infty}^{x} e^{-\frac{t^2}{2}} dt \quad (6b)$$

3 The proposed frequency-domain criterion

Let us consider a point P in the structural component submitted to a general time-varying random stress state. The stress tensor, defined with respect to the fixed frame $PXYZ$ (Fig. 2), is described by the time-varying stress vector $\mathbf{s}_{xyz}(t) = \{s_1, s_2, s_3, s_4, s_5, s_6\}^T = \{\sigma_x, \sigma_y, \sigma_z, \tau_{xy}, \tau_{xz}, \tau_{yz}\}^T$.

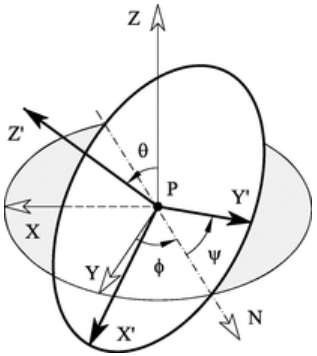

Fig. 2 Reference systems: fixed frame $PXYZ$ and rotated frame $PX'Y'Z'$.

3.1 Definition of the critical plane

By assuming that the random features of the stress tensor can be described by a six-dimensional ergodic stationary Gaussian stochastic process with zero mean values, the matrix of PSD functions, $\mathbf{S}_{xyz}(\omega)$, is expressed as follows:

$$\mathbf{S}_{xyz}(\omega) = \begin{bmatrix} S_{1,1} & S_{1,2} & S_{1,3} & S_{1,4} & S_{1,5} & S_{1,6} \\ S_{2,1} & S_{2,2} & S_{2,3} & S_{2,4} & S_{2,5} & S_{2,6} \\ S_{3,1} & S_{3,2} & S_{3,3} & S_{3,4} & S_{3,5} & S_{3,6} \\ S_{4,1} & S_{4,2} & S_{4,3} & S_{4,4} & S_{4,5} & S_{4,6} \\ S_{5,1} & S_{5,2} & S_{5,3} & S_{5,4} & S_{5,5} & S_{5,6} \\ S_{6,1} & S_{6,2} & S_{6,3} & S_{6,4} & S_{6,5} & S_{6,6} \end{bmatrix} \quad (7)$$

where ω is the pulsation.

If one considers a rotated coordinate system $PX'Y'Z'$ (Fig. 2), defined by the three Euler angles ϕ, θ, ψ, the PSD matrix can easily be computed from the following relationship:

$$\mathbf{S}_{x'y'z'}(\omega) = \mathbf{C}\mathbf{S}_{xyz}(\omega)\mathbf{C}^T \quad (8)$$

where the rotation matrix is $\mathbf{C} = \mathbf{C}(\phi, \theta, \psi)$.

According to the concept adopted in the time-domain criterion [13,14], the critical plane is linked to averaged principal stress directions. Therefore, by varying the angles ϕ, θ, the direction Z' experiencing the maximum $\sigma_{Z'}$ in a statistical sense is

determined:

$$E\left[\max_{0\leqslant t\leqslant T}\sigma_{z'}(t)\right]\cong\sqrt{\lambda_0}\sqrt{2\ln(N_1)}+\frac{0.5772}{\sqrt{2\ln(N_1)}} \tag{9}$$

being T the observation period, and λ_0 the spectral moment of order 0 of the PSD function $S_{3',3'}$. Further: $N_1=\nu_0^+T$, with ν_0^+ the expected rate of mean zero-upcrossings of $\sigma_{z'}$. The angle ψ (and therefore the Y' axis) is made to vary in order to maximise the variance of $\tau_{y'z'}$:

$$\max_{0\leqslant\psi\leqslant2\pi}\left[\sigma^2_{6',6'}\right]=\left[\max_{0\leqslant\psi\leqslant2\pi}\int_{-\infty}^{+\infty}S_{6',6'}(\omega,\psi)d\omega\right] \tag{10}$$

The directions Z' and Y' are regarded as the averaged principal directions $\hat{\bar{1}}$ and $\hat{\bar{3}}$, respectively (Fig. 3).

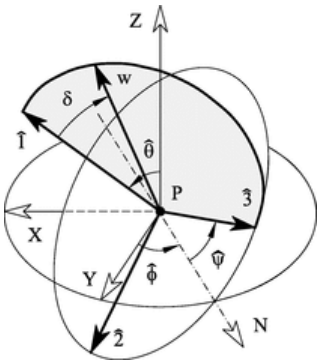

Fig. 3 Averaged principal stress reference system $P\hat{\bar{1}}\hat{\bar{2}}\hat{\bar{3}}$.

Consequently, the direction X' is regarded as the averaged principal direction $\hat{\bar{2}}$.

The normal to the critical plane, $\mathbf{w}$, is defined by the off-angle δ (clockwise rotation) about the axis $\hat{\bar{2}}$ (Fig. 4), where such an off-angle is a function of the ratio between fully reversed shear and normal stress fatigue limits:

$$\delta=\frac{3\pi}{8}\left[1-\left(\frac{\tau_{af,-1}}{\sigma_{af,-1}}\right)^2\right] \tag{11}$$

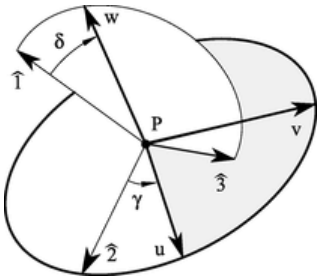

Fig. 4 Reference system attached to the critical plane $Puvw$.

3.2 Definition of the equivalent stress PSD

The frame $Puvw$ is attached to the critical plane (Fig. 4), and the stress tensor at point P related to such a coordinate system is named $\mathbf{s}_{uvw}(t)=\{s_{1''},s_{2''},s_{3''},s_{4''},s_{5''},s_{6''}\}^T=\{\sigma_u,\sigma_v,\sigma_w,\tau_{uv},\tau_{uw},\tau_{vw}\}^T$. The u-axis defines the direction that maximises the variance of the ergodic stationary Gaussian stochastic process $\tau_{vw}=s_{6'',6''}$:

$$\max_{0\leqslant\gamma\leqslant 2\pi}\left[\sigma^2_{6'',6''}\right]=\left[\max_{0\leqslant\gamma\leqslant 2\pi}\int_{-\infty}^{+\infty}S_{6'',6''}(\omega,\gamma)d\omega\right] \tag{12}$$

being the angle γ a counterclockwise rotation about the w -axis.

In order to reduce the multiaxial stress state to an equivalent uniaxial stress state, we propose here to determine an equivalent PSD function through the following linear function:

$$S_{eq}=S_{w,w}+\left(\frac{\sigma_{af,-1}}{\tau_{af,-1}}\right)S_{vw,vw} \tag{13}$$

3.3 Damage estimation and fatigue life

The expected fatigue damage per unit time, $E[D]$, may be evaluated by employing the following linear cumulative damage rule:

$$E[D]=\nu_a C^{-1}\int_0^{+\infty}s^k p_a(s)ds \tag{14}$$

where ν_a is the expected rate of occurrence of loading cycles, k and C are the parameters of the normal stress S-N curve ($s^kN=C$), and $p_a(s)$ is the probability distribution of the amplitude s of the counted equivalent stress cycles. Since Eq. (14) implicitly considers a negligible effect of the equivalent stress mean values on damage, the probability distribution $p_a(s)$ represents the marginal distribution of the bivariate distribution $p_{a,m}(s,m)$, where *m* is the mean value of a counted cycle.

Note that damage estimation in Eq. (14) depends on the algorithm used to count the loading cycles, i.e. it is related to the method adopted to estimate the marginal density $p_a(s)$. The Rain-Flow Counting (RFC) procedure [22] is considered as the most accurate one by the scientific community. Such a procedure is a complete counting procedure, that is, each peak is paired with a lower or equal valley and, therefore, the expected rate of loading cycles is equal to the expected rate of peaks, that is, ν_a in Eq.(14) is equal to ν_p (see Eq.(4)).

For the RFC method, an analytical solution for $p_a^{RFC}(s)$ is not available in the literature and, therefore, the problem of the RFC damage estimation $E[D_{RFC}]$ has been addressed so far in an approximate manner [18,23–25].

Wirsching and Light [23] proposed to correlate the expected fatigue damage rate of the RFC method to that of a narrow-band process $E[D_{NB}]$, namely:

$$E\left[D_{RFC}^{WL}\right]=\chi\cdot E[D_{NB}] \tag{15}$$

where

$$\chi=(0.926-0.033k)+[1-(0.926-0.033k)]\left(1-\sqrt{1-\alpha_2^2}\right)^{1.587k-2.323} \tag{16a}$$

and

$$E[D_{NB}]=\nu_p C^{-1}(\sqrt{2\lambda_0})^k\Gamma\left(1+\frac{k}{2}\right) \tag{16b}$$

with Γ = gamma function ($\Gamma(z)=\int_0^{+\infty}t^{z-1}e^{-t}dt$). Note that, according to the Wirsching and Light approximation, the rain-flow damage depends on the three spectral moments λ_0 , λ_2 and λ_4 .

Dirlik [24] estimated the expected fatigue damage rate of the RFC method (on the basis of an approximate expression for the rain-flow amplitude density), equal to the sum of an exponential and two Rayleigh probability densities:

$$E\left[D_{RFC}^{DK}\right]=\nu_p C^{-1}(\sqrt{\lambda_0})^k\left[D_1Q^k\Gamma(1+k)+(\sqrt{2})^k\Gamma\left(1+\frac{k}{2}\right)\left(D_2|R|^k+D_3\right)\right] \tag{17}$$

where D_1 , D_2 , D_3 , Q and R are fitting parameters dependent on the following four spectral moments: λ_0 , λ_1 , λ_2 and λ_4 .

Zhao and Baker [25] estimated the expected fatigue damage rate of the RFC method (on the basis of an approximate expression for the rain-flow amplitude density) equal to a linear combination of one Weibull and one Rayleigh density:

$$E\left[D_{RFC}^{ZB}\right] = \nu_p C^{-1}(\sqrt{\lambda_0})^k \left[la^{-k/b}\Gamma\left(1+\frac{k}{b}\right) + (1-l)2^{k/2}\Gamma\left(1+\frac{k}{2}\right)\right] \quad (18)$$

where a, b are the Weibull parameters and l is a weighting factor. These coefficients are estimated on the basis of some spectral moments.

Finally, Tovo and Benasciutti [18] estimated the RFC damage by considering a proper intermediate point between the lower and the upper bounds of $E[D_{RFC}]$:

$$E\left[D_{RFC}^{TB}\right] = b \cdot E[D_{NB}] + (1-b) \cdot E[D_{RC}] \quad (19)$$

being $b = (\alpha_{0.75}^2 - \alpha_2^2)/(1-\alpha_2^2)$. The lower bound of RFC damage, $E[D_{RC}]$, is related to range-mean cycle counting, and can approximately be estimated as follows (e.g. see Ref. [18]):

$$E[D_{RC}] \cong \nu_p C^{-1}(\sqrt{2\lambda_0}\alpha_2)^k \Gamma\left(1+\frac{k}{2}\right) = E[D_{NB}]\alpha_2^{k-1} \quad (20)$$

The above approximate expressions of the RFC fatigue damage (see Eqs. (15), (17)–(19)) are implemented in the criterion here proposed in order to assess how the estimation of the rain-flow distribution influences fatigue life. Note that fatigue damage rate is constant in a stationary process and, considering a critical damage equal to the unity, the calculated fatigue life is given by:

$$T_{cal} = \frac{1}{E[D_{RFC}]} \quad (21)$$

4 Frequency-domain based criterion validation

The criterion is applied to some relevant random fatigue experimental results available in the literature [26], related to smooth specimens made of 18G2A and 10HNAP steels. The fatigue properties of the above materials are reported in Table 1, where $\sigma_{af,-1}$, N_0, C and k are the material parameters related to the S–N curve for fully reversed bending, whereas $\tau_{af,-1}$ is obtained from the S–N curve for fully reversed torsion.

Table 1 Fatigue properties for each examined material.

Material	$\sigma_{af,-1}$ [MPa]	N_0 [cycles]	C [MPa^k]	k	$\tau_{af,-1}$ [MPa]
18G2A	270	2.375 (10)^6	7.61 (10)^{23}	7.20	170
10HNAP	300	3.135 (10)^6	6.63 (10)^{30}	9.82	182

For both examined materials, the specimens were submitted to non-proportional random bending ($\sigma = \sigma_x$) and torsion ($\tau = \tau_{xy}$) stresses with zero mean values [26]. The random loadings had a dominant frequency of 28.8 Hz for bending and 30 Hz for torsion. The loading histories were independent; further, they were sums of four harmonic components with different amplitudes (following a Gaussian probability distribution) and phases. The loading histories had a duration of 820 s and a sampling frequency of 500 Hz.

In such tests, 13 combinations of normal and shear stress loading histories characterised by different values of the ratio τ_{max}/σ_{max}, ranging from 0.189 to 0.840, were analysed. The 13 loading combinations for each examined material are processed by means of the proposed criterion (using the different narrow-band approximations being presented) based on a frequency-domain approach (accordingly, the criterion takes into account the loading conditions through the discrete spectra obtained from the FFT of the experimentally recorded stress time histories).

As an example, the PSD functions S_σ and S_τ of the applied stress components related to the experimental tests characterised by τ_{max}/σ_{max} equal to 0.19, 0.50 and 0.84 are shown in Figs. 5–7, respectively. It can be noted that such PSD functions are characterised by four frequency peaks.

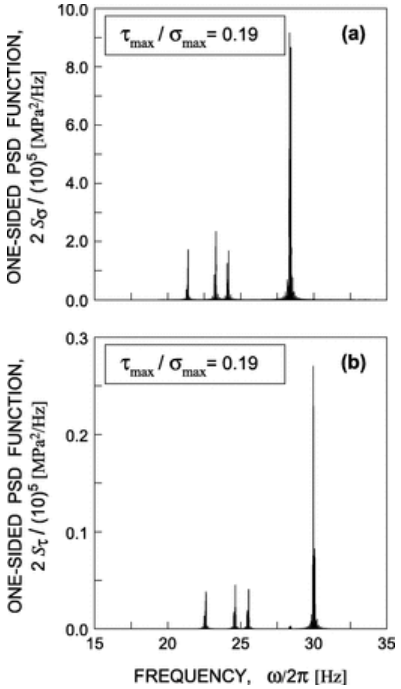

Fig. 5 PSD functions of the applied loading: (a) bending and (b) torsion random stresses with $\tau_{max}/\sigma_{max} = 0.19$.

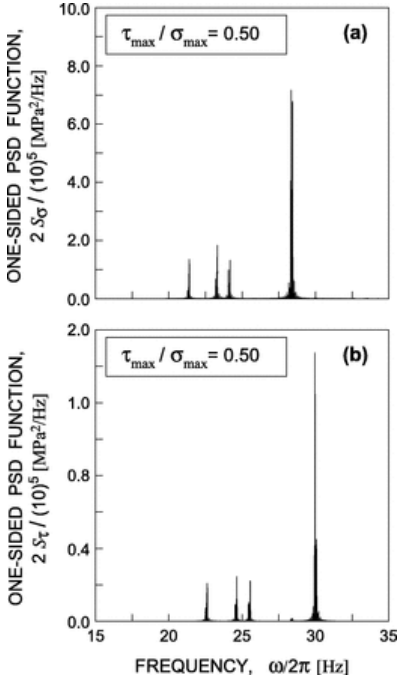

Fig. 6 PSD functions of the applied loading: (a) bending and (b) torsion random stresses with $\tau_{max}/\sigma_{max} = 0.50$.

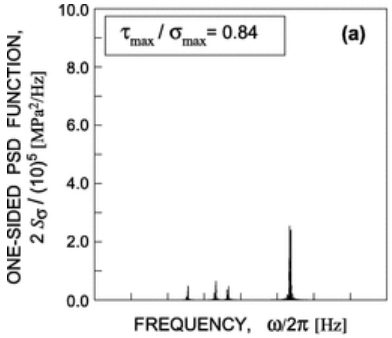

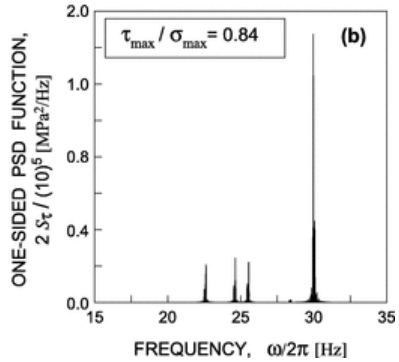

Fig. 7 PSD functions of the applied loading: (a) bending and (b) torsion random stresses with $\tau_{max}/\sigma_{max} = 0.84$.

In Fig. 8, the PSD functions of the equivalent stress S_{eq} for the above loading combinations are reported for both 18G2A steel (Fig. 8(a), (c), (e)) and 10HNAP steel (Fig. 8(b), (d), (f)). By comparison with the plots in Figs. 5–7, the PSD functions S_{eq} in Fig. 8 presents in general 8 peaks in correspondence to the dominant frequencies of the spectra of the applied stress components.

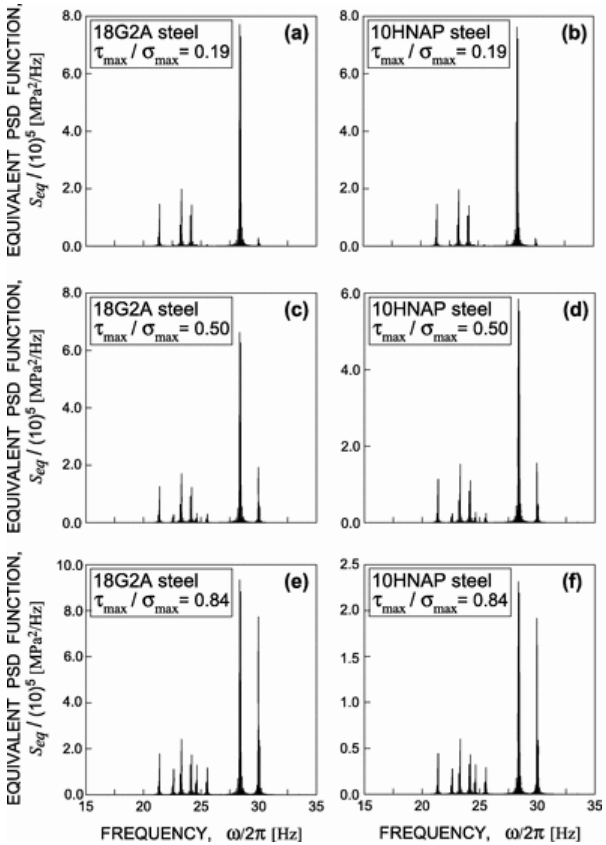

Fig. 8 PSD function S_{eq} for tests on 18G2A and 10HNAP steels characterised by a τ_{max}/σ_{max} ratio equal to: (a)–(b) 0.19, (c)–(d) 0.50, (e)–(f) 0.84.

The comparison between experimental and theoretical predictions both for 18G2A and 10HNAP steels is shown in Figs. 9 and 10, respectively, where the solid line indicates $T_{cal} = T_{exp}$, the dashed lines correspond to T_{cal}/T_{exp} equal to 0.5 and 2, and the dash-dot lines correspond to T_{cal}/T_{exp} equal to 0.3 and 3, with the T_{cal} values determined by alternatively applying the above models to estimate the marginal density $p_a(s)$ [18,23–25].

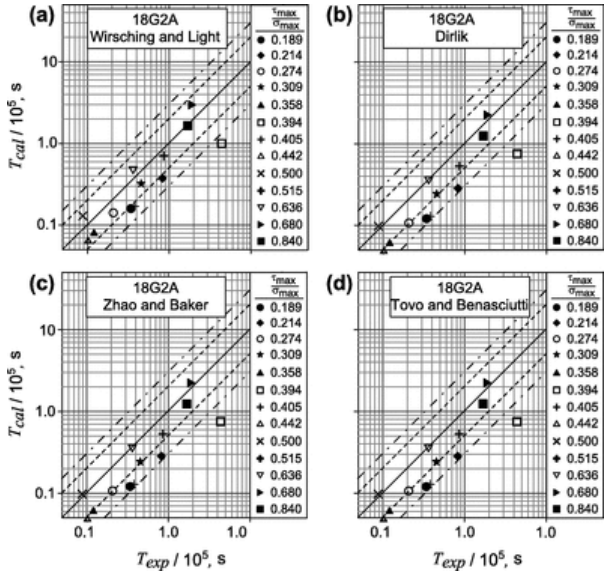

Fig. 9 Comparison between calculated and experimental fatigue lives for 18G2A steel, by applying the proposed criterion and: (a) the Wirsching and Light model [21], (b) the Dirlik model [22], (c) the Zhao–Baker model [23], (d) the Tovo and Benasciutti model [17].

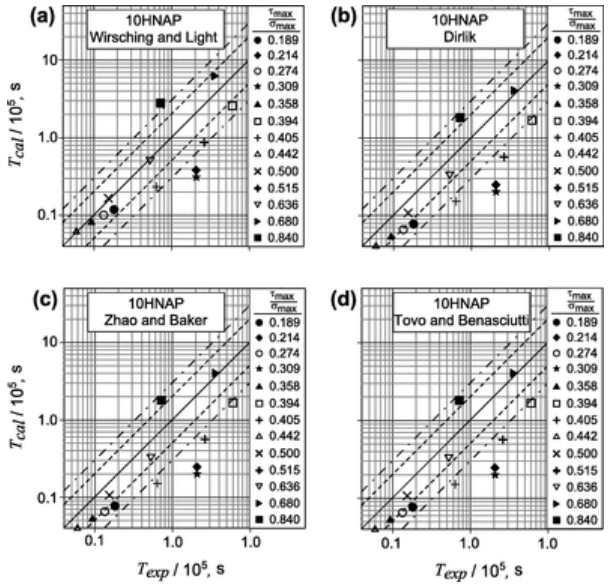

Fig. 10 Comparison between calculated and experimental fatigue lives for 10HNAP steel, by applying the proposed criterion and: (a) the Wirsching and Light model [21], (b) the Dirlik model [22], (c) the Zhao–Baker model [23], (d) the Tovo and Benasciutti model [17].

A good agreement for the fatigue loading being examined can be noticed especially by applying the Wirsching and Light model (see Tables 2 and 3, where scatter 2 stands for the percentage of results satisfying $0.5 \leqslant T_{cal}/T_{exp} \leqslant 2.0$, and scatter 3 stands for the percentage of results satisfying $0.3 \leqslant T_{cal}/T_{exp} \leqslant 3.0$), whereas equal results are achieved with the other methods.

Table 2 Summary for 18G2A steel of the comparison in terms of experimental and estimated lifetime for different narrow-band approximations.

Model	Ref.	SCATTER 2 [%]	SCATTER 3 [%]
Wirsching and Light	[21]	69	92
Dirlik	[22]	54	92
Zhao and Baker	[23]	54	92
Tovo and Benasciutti	[17]	54	92

Table 3 Summary for 10HNAP steel of the comparison in terms of experimental and estimated lifetime for different narrow-band approximations.

Model	Ref.	Scatter 2 [%]	Scatter 3 [%]
Wirsching and Light	[21]	54	77
Dirlik	[22]	46	69
Zhao and Baker	[23]	46	69
Tovo and Benasciutti	[17]	46	69

5 Frequency-domain criterion against time-domain criterion

The theoretical results determined by applying the above frequency-domain criterion are here compared with those obtained through the time-domain criterion proposed in the past by some of the present authors [13,14].

Now some basic concepts related to the above time-domain criterion are briefly outlined. Then, a comparison between experimental and theoretical fatigue lives is performed, the latter being evaluated through both the reformulated frequency-domain criterion and the time-domain criterion reported in Refs. [13,14].

5.1 Time-domain criterion

The main aspects of the time-domain criterion published in Refs. [13,14] are presented here. The critical plane is assumed to be connected to the mean directions $\hat{1}, \hat{2}$ and $\hat{3}$ of the principal stress axes. Such directions are obtained from averaging the instantaneous values of the principal Euler angles through a weight function which depends on two parameters deduced from the S–N curve for fully reversed bending.

The stress vector $\mathbf{Sw}$ $\mathbf{S}_w$ related to the critical plane orientation is decomposed in normal stress component $\mathbf{N}$ (perpendicular to the critical plane) and shear stress component $\mathbf{C}$ (lying on the critical plane). The scalar value of the vector $N(t)$ is taken as the cycle counting variable. The sequence N_i is reduced by eliminating the time instants corresponding to non-extreme values. The same time instants are also eliminated in the sequence C_i. By using the rainflow method, the amplitude of an equivalent normal stress is evaluated by the following expression, for each z -th resolved reversal:

$$\sigma_{eq,a,z} = \sqrt{(N^*_{\max,z})^2 + \left(\frac{\sigma_{af,-1}}{\tau_{af,-1}}\right)^2 (C^*_{a,z})^2} \tag{22}$$

Using a nonlinear cumulative damage rule for $\sigma_{eq,a,z}$ [28], the total damage at time T_0 is obtained as follows:

$$D(T_0) = \sum_{z=1}^{Z} (D_z)^q \tag{23a}$$

with:

$$D_z = \begin{cases} \dfrac{1}{2N_0 \left(\frac{\sigma_{af,-1}}{\sigma_{eq,a,z}}\right)^k} & \text{for } \sigma_{eq,a,z} \geqslant c\sigma_{af,-1} \\ 0 & \text{for } \sigma_{eq,a,z} \leqslant c\sigma_{af,-1} \end{cases} \tag{23b}$$

and

$$q = 1 + \frac{0.25}{(1-c)\sigma_{af,-1}}(\sigma_{eq,a,z} - \sigma_{af,-1}) \tag{23c}$$

The symbol Z refers to the total number of reversals at time instant T_0. Moreover, N_0 is the number of cycles at fatigue limit, $\sigma_{af,-1}$ and k are parameters obtained from the $S-N$ curve being considered, and c is a safety coefficient, $0 \leqslant c < 1$ (c is assumed to be equal to 0.5).

Finally, the calculated fatigue life of the structural component examined is given by the following expression:

$$T_{cal} = \frac{T_0}{D(T_0)} \tag{24}$$

5.2 Fatigue life results

The above time-domain criterion is here applied to the experimental data [26] reported in Section 4. The comparison between experimental data, T_{exp}, and theoretical fatigue life, T_{cal}, is shown in Fig. 11(a) and (b) for 18G2A and 10HNAP steels, respectively. In particular, the following remarks can be made:

- for 18G2A steel (Fig. 11(a)), 31% of fatigue life calculation results are included into 2x band, whereas 54% of such results are included into 3x band;
- for 10HNAP steel (Fig. 11(b)), 23% of fatigue life calculation results are included into 2x band, whereas 38% of such results are included into 3x band.

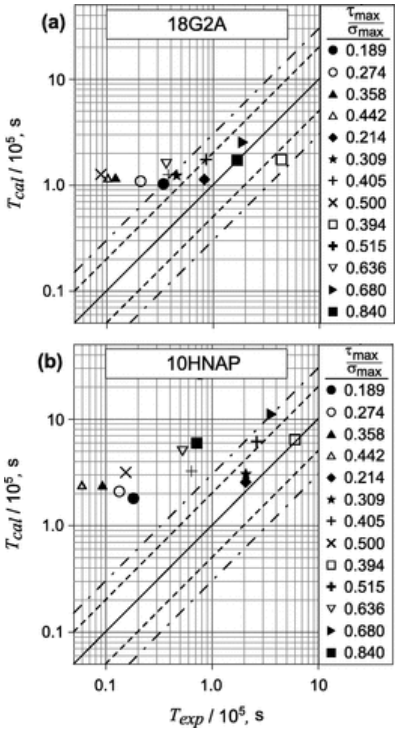

Fig. 11 Comparison between experimental and calculated fatigue lives, determined by employing the time-domain criterion reported in Refs. [13,14] for: (a) 18G2A steel, (b) 10HNAP steel.

Then, the above results are compared with those determined by implementing the Wirsching and Light model in the reformulated frequency-domain criterion, since most accurate results are achieved employing such a model. In order to perform such a comparison from a statistical point of view, the root mean square error method is used [29]. The value of the root mean square logarithmic error is computed as follows:

$$E_{RMS} = \sqrt{\frac{\sum_{i=1}^{n} \log^2\left(\frac{T_{exp,i}}{T_{calc,i}}\right)}{n}} \tag{25}$$

where n is the total number of the examined loading combinations. Finally, the mean square error T_{RMS} is given by:

$$T_{RMS} = 10^{E_{RMS}} \tag{26}$$

Fig. 12 shows the mean square error computed by alternatively applying both criteria (in time-domain or frequency-domain) for each tested material. The comparison clearly proves that better estimations are derived by applying the reformulated frequency-domain criterion, being the value of T_{RMS} equal to about 1.87 for 18G2A steel and 2.59 for 10HNAP steel.

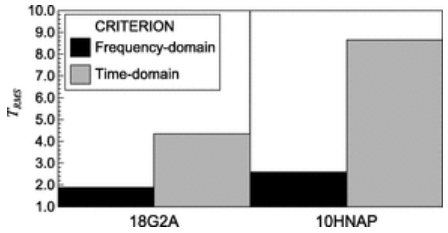

Fig. 12 Mean square error for both the frequency-domain criterion (by implementing the Wirsching and Light model) and the time domain criterion [13,14], for each examined structural steel.

6 Conclusions

A frequency-domain critical-plane criterion has been here reformulated in order to improve the accuracy in fatigue life evaluation for smooth metallic structural components under multiaxial random loading.

The critical plane orientation has been determined through the PSD matrix of the stress tensor. Then, an equivalent PSD function has been defined and processed through some damage models in order to compute the fatigue lifetime of the structural component being examined.

The comparison with some experimental tests related to smooth specimens made of 18G2A and 10HNAP structural steels has been satisfactory. Finally, the capabilities of the present criterion have been highlighted by comparing, from a statistical point of view, the above theoretical results with those determined by employing a time-domain criterion proposed in the past by some of the authors.

Acknowledgements

The authors gratefully acknowledge the financial support of the Italian Ministry of Education, University and Research (MIUR).

References

[1]

M. Mršnik, J. Slavič and M. Boltežar, Frequency-domain methods for a vibration-fatigue-life estimation – application to real data, *Int J Fatigue* **47**, 2013, 8–17.

[2]

S.H. Han, D.G. An, S.J. Kwak and K.W. Kang, Vibration fatigue analysis for multi-point spot-welded joints based on frequency response changes due to fatigue damage accumulation, *Int J Fatigue* **48**, 2013, 170–177.

[3]

B. Echard, N. Gayton and A. Bignonnet, A reliability analysis method for fatigue design, *Int J Fatigue* **59**, 2014, 292–300.

[4]

G. Marsh, C. Wignall, P.R. Thies, N. Barltrop, A. Incecik, V. Venugopal, et al., Review and application of Rainflow residue processing techniques for accurate fatigue damage estimation, *Int J Fatigue* **82**, 2016, 757–765.

[5]

A. Niesłony, M. Růžička, J. Papuga, A. Hodr, M. Balda and J. Svoboda, Fatigue life prediction for broad-band multiaxial loading with various PSD curve shapes, *Int J Fatigue* **44**, 2012, 74–88.

[6]

T.X. Xia and W.X. Yao, Comparative research on the accumulative damage rules under multiaxial block loading spectrum for 2024-T4 aluminum alloy, *Int J Fatigue* **48**, 2013, 257–265.

[7]

Z. Marciniak, D. Rozumek and E. Macha, Verification of fatigue critical plane position according to variance and damage accumulation methods under multiaxial loading, *Int J Fatigue* **58**, 2014, 84–93.

[8]

A. Hor, N. Saintier, C. Robert, T. Palin-Luc and F. Morel, Statistical assessment of multiaxial HCF criteria at the grain scale, *Int J Fatigue* **67**, 2014, 151–158.

[9]

J. Ge, Y. Sun and S. Zhou, Fatigue life estimation under multiaxial random loading by means of the equivalent Lemaitre stress and multiaxial S–N curve methods, *Int J Fatigue* **79**, 2015, 65–74.

[10]

Y. Wang and L. Susmel, The modified Manson–Coffin curve method to estimate fatigue lifetime under complex constant and variable amplitude multiaxial fatigue loading, *Int J Fatigue* **83**, 2016, 135–149.

[11]

C.H. Wang and M.W. Brown, Life prediction techniques for variable amplitude multiaxial fatigue – part 1: theories, *J Eng Mater Technol* **118**, 1996, 367–370.

[12]

T. Łagoda, E. Macha, A. Niesłony and A. Muller, Comparison of calculation and experimental fatigue lives of some chosen cast irons under combined tension and torsion, In: M. Fuentes, et al., (Eds.), *Proceedings of ECF13 – application and challenges,* 2000, Elsevier; San Sebastian, 6.

[13]

A. Carpinteri, A. Spagnoli and S. Vantadori, A multiaxial fatigue criterion for random loading, *Fatigue Fract Eng Mater Struct* **26**, 2003, 515–522.

[14]

A. Carpinteri, A. Spagnoli and S. Vantadori, Fatigue life estimation under multiaxial random loading using a critical plane-based criterion, In: *Proceedings of the 2nd international conference on material and component performance under variable amplitude loading, Darmstadt,* 2009, 475–484.

[15]

X. Pitoiset and A. Preumont, Spectral methods for multiaxial random fatigue analysis of metallic structures, *Int J Fatigue* **22**, 2000, 541–550.

[16]

T. Łagoda, E. Macha and A. Niesłony, Fatigue life calculation by means of the cycle counting and spectral methods under multiaxial random loading, *Fatigue Fract Eng Mater Struct* **28**, 2005, 409–420.

[17]

E. Macha, T. Łagoda, A. Niesłony and D. Kardas, Fatigue life under variable-amplitude loading according to the cycle-counting and spectral methods, *Mater Sci* **42**, 2006, 416–425.

[18]

D. Benasciutti and R. Tovo, Comparison of spectral methods for fatigue analysis in broad-band Gaussian random processes, *Probab Eng Mech* **21**, 2006, 287–299.

[19]

J. Ge, Y. Sun, S. Zhou, L. Zhang, Y. Zhang and Q. Zhang, A hybrid frequency–time domain method for predicting multiaxial fatigue life of 7075-T6 aluminium alloy under random loading, *Fatigue Fract Eng Mater Struct* **38**, 2014, 247–256.

[20]

A. Carpinteri, A. Spagnoli and S. Vantadori, Reformulation in the frequency domain of a critical plane-based multiaxial fatigue criterion, *Int J Fatigue* **67**, 2014, 55–61.

[21]

Y. Jiang, W. Ott, C. Baum, Michael Vormwald and H. Nowack, Fatigue life predictions by integrating EVICD fatigue damage model and an advanced cyclic plasticity theory, *Int J Plasticity* **25**, 2009, 780–801.

[22]

Standard Practices for Cycle Counting in Fatigue Analysis. ASTM E 1049; 1990.

[23]

P.H. Wirsching and C.L. Light, Fatigue under wide band random stresses, *J Struct Div ASCE* **106**, 1980, 1593–1607.

[24]

T. Dirlik, Application of computers in fatigue analysis, PhD thesis1985, University of Warwick; UK.

[25]

W. Zhao and M.J. Baker, On the probability density function of Rainflow stress range for stationary Gaussian processes, *Int J Fatigue* **14**, 1992, 121–135.

[26]

Z. Marciniak, D. Rozumek and E. Macha, Fatigue lives of 18G2A and 10HNAP steels under variable amplitude and random non-proportional bending with torsion loading, *Int J Fatigue* **30**, 2008, 800–813.

[27]

S.K. Paul, Prediction of non-proportional cyclic hardening and multiaxial fatigue life for FCC and BCC metals under constant amplitude of strain cycling, *Mater Sci Eng, A* **656**, 2016, 111–119.

[28]

J. Cacko, Simultaneous computer simulation of operational random processes and continual Rainflow counting, *Int J Fatigue* **14**, 1992, 183–188.

[29]

K. Walat and T. Łagoda, Lifetime of semi-ductile materials through the critical plane approach, *Int J Fatigue* **67**, 2014, 73–77.

Highlights

- A frequency-domain criterion based on the critical plane is reformulated.
- The critical plane is dependent on the PSD matrix of the stress tensor.
- The PSD of an equivalent stress is used to estimate fatigue damage.
- Different damage models are implemented in the frequency-domain criterion.
- Comparisons with experimental and time-domain criterion results are satisfactory.

Queries and Answers

Query: Your article is registered as a regular item and is being processed for inclusion in a regular issue of the journal. If this is NOT correct and your article belongs to a Special Issue/Collection please contact m.venkatesan@elsevier.com immediately prior to returning your corrections.
Answer: Correct

Query: The author names have been tagged as given names and surnames (surnames are highlighted in teal color). Please confirm if they have been identified correctly.

elsevier_JIJF_3956

Answer: Correct